MOCVD growth of InGaAs metamorphic heterostructures for photodiodes with low dark current

© I.V. Samartsev, B.N. Zvonkov, N.V. Baidus, A.B. Chigineva, K.S. Zhidyaev, N.V. Dikareva, A.V. Zdoroveyshchev, A.V. Rykov, S.M. Plankina, A.V. Nezhdanov, A.V. Ershov

Lobachevsky State University,
603022 Nizhny Novgorod, Russia

E-mail: samartsev@nifti.unn.ru

Received May 30, 2023
Revised June 20, 2023
Accepted July 17, 2023

The epitaxial growth technique of InGaAs photodiode structures based on a digital InGaAs/GaAs metamorphic buffer layer by metalorganic chemical vapor deposition has been developed. The spectral dependence of the photocurrent of photodiodes based on the produced structures has a maximum at the $1.24\,\mu$m wavelength. The photosensitivity range at 10% of peak is $1.17-1.29\,\mu$m at room temperature. The current-voltage characteristics in the temperature range $9-300\,$K were investigated. It is shown that the dark current consists of generation-recombination and tunneling components. The dark current density at room temperature was $8 \cdot 10^{-5}\,$A/cm^2 with a reverse bias of $-5\,$V

Keywords: MOCVD, nanomaterials, semiconductors $A^{III}B^{V}$, infrared photodiodes, dark current.

DOI: 10.61011/SC.2023.06.57171.4964

1. Introduction

Photodiodes operating in the wavelength range $\sim 1.3\,\mu$m are widely used in fiber-optic communication lines (fiber optic lines), rangefinder systems and other radiation detection systems. *p-i-n*-structures based on a solid solution $In_xGa_{1-x}As$ with a high In content grown on an InP substrate are now most often used to create detectors for this range. However, InP substrates, due to their mechanical properties, are less amenable to post-processing technology than gallium arsenide. InP substrates have a smaller diameter, which reduces the number of chips obtained from the plate in the technological process. In addition, InP substrates are expensive. Thus, the replacement of indium phosphide substrates with GaAs for photodiodes at wavelengths $\sim 1.3\,\mu$m is very relevant.

Currently, a common approach to creating mismatched $A^{III}B^{V}$ structures is the use of metamorphic buffer (MB) layers of variable composition for a smooth or stepwise change in the lattice parameter. It is known that the implementation of metamorphic structures on gallium arsenide, the transport and structural characteristics of which would not be inferior to those of InP structures, is difficult due to the appearance of a microrelief of the surface and incomplete suppression of dislocations sprouting into the active layers of the structure [1]. Dislocation filters in the form of stressed superlattices [2] are often used to reduce the dislocation density, but strict requirements of high crystal quality are imposed on the layers of such a filter. Otherwise, the superlattice itself can additionally introduce both point defects and dislocations penetrating into the photosensitive area of the instrument structures. The authors of the work [3] demonstrated a metamorphic $In_xGa_{1-x}As$-converter of laser radiation at a wavelength of $1.064\,\mu$m, the density of dislocations in the photosensitive region of which was $3 \cdot 10^{16}\,$cm^{-2}. However, to achieve large wavelengths, an increase in the concentration of In in a solid solution of $In_xGa_{1-x}As$ is required, which will lead to an increase in mismatch with the substrate and an increase in the density of dislocations in the photosensitive region. [4,5] reported about detectors at a wavelength of $> 1\,\mu$m grown on GaAs substrates with $In_xGa_{1-x}As$ MB layer with a stepwise change in composition. Unfortunately, these structures showed a high dislocation density ($1.5 \cdot 10^7\,$cm^{-2}) and significant dark currents, even in cases when the thickness of the buffer layers reached several micrometers. Thus, the search for methods for the formation of metamorphic structures remains relevant in order to increase the crystal perfection of epitaxial layers, as well as to expand the working range of photodiodes into the long-wavelength region.

To this end, in a number of works [6–11] attempts were made to create MB layers in photosensitive structures using the method of molecular beam epitaxy (MBE). For example, the authors of [6] managed to create photosensitive structures on an InP substrate with digital MB and an indium content of 83% in the active region using this method. However, the method of MOCVD is used for the formation of most commercially produced semiconductor devices, and the creation of photodetectors for mass electronics poses the task of obtaining heterostructures on GaAs substrates by this method.

A modified method of forming a digital MB on a GaAs substrate by the method of MOCVD is considered in this paper to create photodiodes for the spectral range $1.0-1.3\,\mu$m.

2. Sample preparation and experiment procedure

The investigated photodiode heterostructures were obtained by the MOCVD method at atmospheric pressure in a horizontal reactor. Layers doped with silicon up to $n = 10^{18}\,\text{cm}^{-3}$ were grown on a *n*-GaAs substrate: buffer *n*-GaAs with a thickness of $0.18\,\mu$m and discrete MB with a total thickness of $1.3\,\mu$m. Then *p-i-n* was formeda structure consisting of layers *n*-$In_{0.3}Ga_{0.7}As$:Si $1.68\,\mu$m thick ($n \sim 10^{18}\,\text{cm}^{-3}$), *i*-$In_{0.3}Ga_{0.7}As$ $0.015\,\mu$m thick and *p*-$In_{0.3}Ga_{0.7}As$:Zn $1.4\,\mu$m thick ($p \sim 7 \cdot 10^{17}\,\text{cm}^{-3}$). The thickness of the layers was calculated based on the growth rate and time, which were obtained based on the study of pre-grown test layers with the same composition. The composition of the test layers was determined by X-ray diffractometry.

The process of forming a digital metamorphic buffer consisted in changing the thicknesses of alternating pairs of GaAs and InGaAs materials in opposite directions as the buffer layer grew, while the composition of the layers remained the same. Thus, at the initial stage of thickness growth, GaAs and $In_{0.3}Ga_{0.7}As$ were 62 and 3 nm, respectively. The thickness of GaAs decreased with the growth of the buffer layer and the thickness of $In_{0.3}Ga_{0.7}As$ increased. The thickness of the GaAs layer was 3 nm at the final stage of MB growth, and the thickness of $In_{0.3}Ga_{0.7}As$ was 62 nm. There are a total of 38 alternating layers. As a result, the digital MB consisted of a set of $GaAs/In_xGa_{1-x}As$ periods of various thicknesses, in which the propagation of dislocations on heterointerfaces should be blocked. The diagram of the design of the heterostructure with MB is shown in Figure 1.

The structural and morphological properties and surface quality of the grown structures were monitored by atomic force microscopy (AFM) using NT-MDT Solver HV facility. The density of dislocations in the surface layer was estimated by the density of pits detected by selective chemical liquid etching and optical microscopy. Photoluminescence spectroscopy (PL) was used to perform the optical quality control of heterostructures. A continuous laser with $\lambda = 0.8\,\mu$m, or a parametric light generator ($\lambda = 0.8\,\mu$m, 10 ns pulse duration, 10 Hz pulse repetition rate) was used to excite the PL. The PL signal was collected from the sample surface when registering stationary spectra PL under conditions of weak pumping (power density $\sim 6\,\text{W/cm}^2$) and from the end of the structure under conditions of pulsed excitation (power density from 50 to 750 kW /cm^2). Acton 2300i lattice monochromator and a multichannel photodetector based on the InGaAs photodiode line (spectral range $0.6-2.2\,\mu$m) were used to record the PL signal.

The Raman scattering (RS) spectra from the cleaved edge cross section (plane (110)) of the structure with MB were analyzed using the NTEGRA SPECTRA (NT-MDT) facility at room temperature using a laser with a wavelength of 473 nm to study the composition of the photosensitive region and the crystal quality of the metamorphic buffer. The radiation was focused by a 100x lens with an aperture of NA = 0.95 into a spot with a diameter of $\sim 1\,\mu$m, the beam power was $\sim 0.5\,\mu$W. Lateral scanning the cleaved surface of the photosensitive structure was carried out with a step of 56 nm from the surface along the direction of growth of the structure [001]. The diameter of the laser beam at half of the intensity distribution, which determines the spatial resolution of the method, was ~ 300 nm [12].

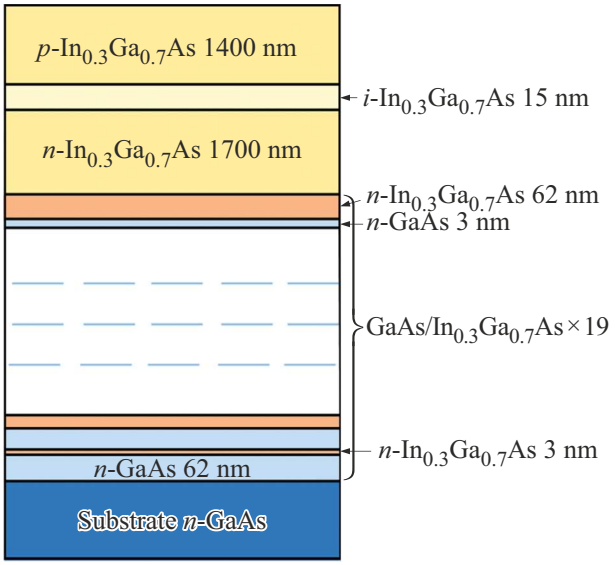

Figure 1. The diagram of a photodiode heterostructure based on a digital MB layer. (A color version of the figure is provided in the online version of the paper).

Laboratory samples of photodiodes were made on the basis of the grown MB heterostructures. To do this, an ohmic Ti/Pd/Au contact was applied from the side of the structure by thermal evaporation in vacuum, and then mesastructures with a diameter of 0.56 mm were formed by precision chemical etching. Cleaning and passivation of the sample surface by reactive ion etching followed by thermal annealing was used to reduce the impact of surface leakage currents.

Dark currents and spectral dependences of the photocurrent were measured on the obtained photodiode samples. The temperature dependences of the volt-ampere characteristics (VAC) of the samples were studied to determine the nature of the dark current. The VAC was measured in a closed-cycle cryostat Janis CCS 300S/202 in the temperature range 9–300 K.

3. Results and discussion

The dislocation density in the surface layer was $10^6\,\text{cm}^{-2}$ on the formed GaAs/MB/InGaAs heterostructures. This value exceeds the dislocation density of the substrates used in the experiment by only 2 orders of magnitude,

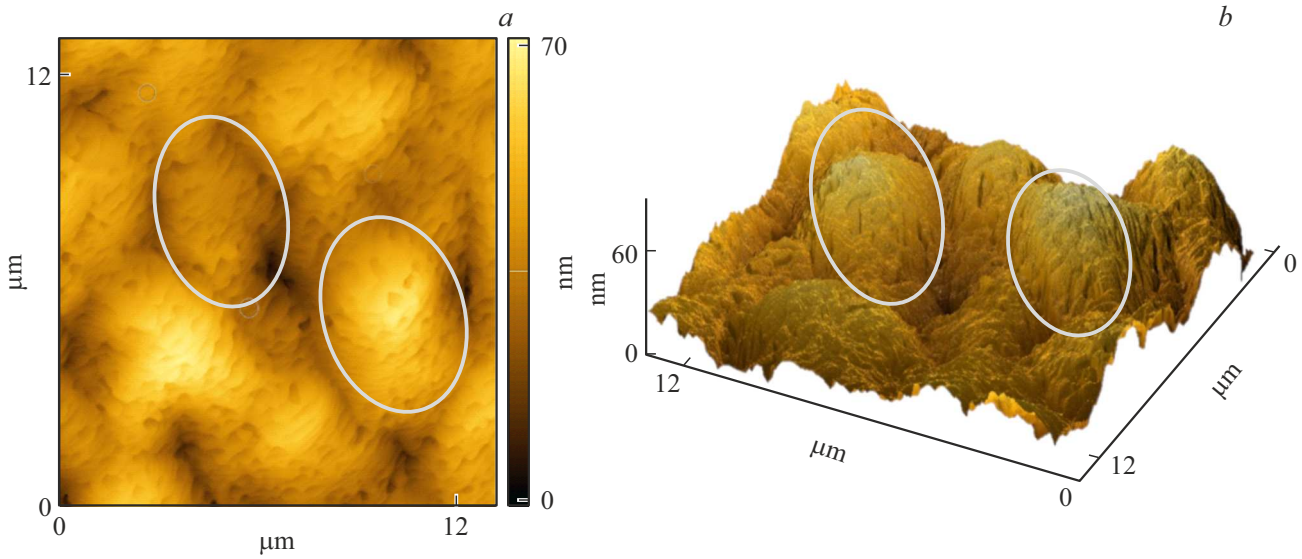

Figure 2. *a* — typical AFM topogram of the structure; *b* — 3D AFM image of the structure surface.

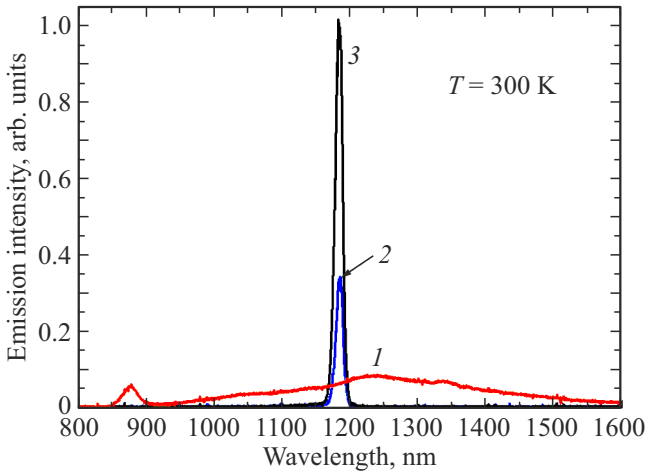

Figure 3. The PL spectra of the structure when pumped by continuous laser radiation (*1*) and pulsed pumping (*2, 3*).

which, according to the literature data, is a good result for structures with MB layers. Figure 2 shows typical AFM images of the grown photodiode structure. The dimensions of the studied site $12 \times 12\,\mu$m. The root mean square error (RMS) of the heights of the irregularities was 20 nm. It can be seen that the surface of the sample has irregularities elongated along the direction [110]. Such relief is observed on the surface of the entire structure and is caused by the generation of a periodic field of mechanical stresses arising as the discrete MB layer grows, and stress relaxation along the most energetically favorable direction [13].

Figure 3 shows a typical PL spectrum of a sample of the structure under study at room temperature. The maximum intensity is observed at a wavelength of 1231 nm under weak pumping conditions (Figure 3, curve *1*). Under high-power pulsed pumping conditions at an exciting radiation density of 250 kW/cm^2, a narrow ($\Delta\lambda < 12$ nm) intense line appears in the radiation spectrum of the sample at a wavelength of 1183nm (Figure 3, curve *2*). An increase in the intensity of the PL by 3 times was recorded with an increase in the power density of the exciting radiation by 1.3 times (Figure 3, curve *3*). Emission lines *2* and *3* (Figure 3) are observed when collecting radiation from the end of the heterostructure and are not expressed when observing PL from the sample surface. This fact, as well as the small width of these lines (~ 12 nm) are signs of stimulated radiation, which indicates the high crystal quality of the photosensitive region of the *p-i-n*-structure.

RS spectra from the (110) surface of the cleaved sample (Figure 4) indicate a monocrystalline structure of epitaxial layers. The approximation of the RS spectra by the Lorentz function reveals the phonon modes of the InGaAs solid solution: a strongly broadened low-intensity InAs-like mode and a closely spaced GaAs-like mode and a DATO mode (disorder activated transverse optical mode [14]) with a comparable intensity. The mode corresponding to GaAs transverse optical phonons (TO-mode) is observed only in the region of the metamorphic buffer and substrate. In addition to the above permitted modes, a low-intensity GaAs-like longitudinal optical (LO) is detected that is prohibited in this geometry fashion.

The frequency position and intensity of the phonon modes depend on the scanning coordinate (Figure 5). In weakly doped regions, the frequency position of the phonon modes of the InGaAs solid solution varies slightly and is 230, 251, 260, 277 cm^{-1} for an InAs-like TO-mode, DATO, GaAs-like TO- and LO-modes, respectively (curves *5, 4, 3, 2*). This frequency value corresponds to the indium content in InGaAs $\sim 30\%$ [14]. A decrease of the frequency of the main modes (GaAs-like TO-mode from

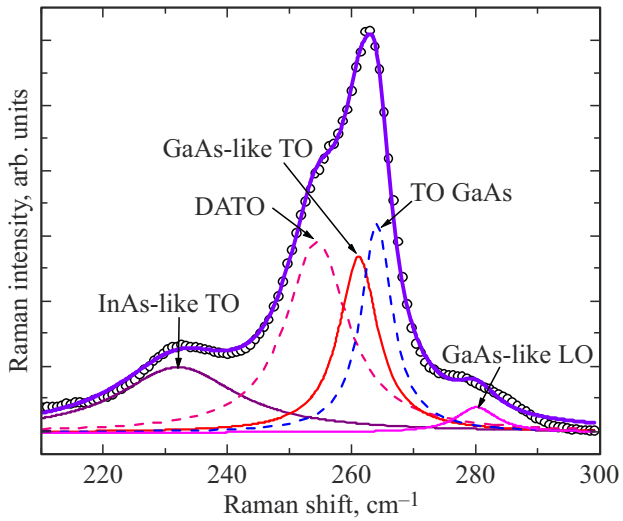

Figure 4. Approximation by the Lorentz function of the Raman spectra from the cleaved surface of the structure in the region of the metamorphic buffer.

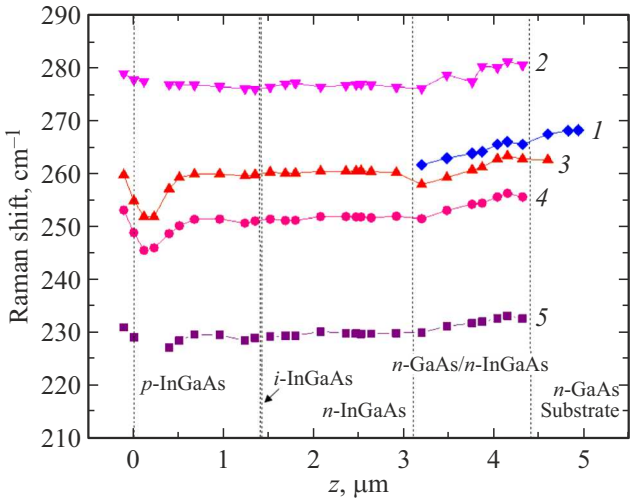

Figure 5. Dependence of the frequency position of phonon modes on the scanning coordinate z: TO-modes GaAs (*1*), GaAs-like modes (*2–4*) and InAs-like modes of solid InGaAs solution (*5*).

260 to 252 cm^{-1}) is observed in the strongly zinc-doped p-region. The low-frequency shift is presumably associated with the appearance of local tensile stresses as a result of embedding Zn into the lattice of a solid solution InGaAs.

A high-frequency shift of all modes of the solid solution (compared with the weakly doped InGaAs region) is observed in the MB region and a low-frequency shift of the GaAs mode from 268 cm^{-1} in the substrate to 262 cm^{-1} at the boundary with p-i-n by the InGaAs transition. This frequency variation corresponds to the tensile stresses in GaAs layers and compression stresses in InGaAs [14] layers. Consequently, the metamorphic buffer is in a stressed state.

It should be noted that the transverse mode from InAs (218.8 cm^{-1}) was not detected, and the intensity of the GaAs mode in MB gradually decreases in accordance with the decrease of the thickness of the layers. This indicates the absence of spinodal decomposition of InGaAs solid solution in the MB region, which is often found in stressed layers of [15,16].

Photodiodes with a diameter and depth of the mesastructure of 560 and 1.5 μm, respectively, were made based on the studied heterostructures and their characteristics were studied. Figure 6 shows a typical spectral dependence of the external quantum output of photodiodes measured at room temperature. The photodiodes had a photosensitivity range of 1.17–1.29 μm at the level of 10% of the maximum at the wavelength of 1.24 μm. Figure 6 shows that the photodiode has no sensitivity at a wavelength of $< 1.15\,\mu$m, which is apparently connected with a small contribution to the photocurrent from absorption at these wavelengths, since measurements of the spectral dependence of the external quantum output were carried out at low power of the exciting radiation.

This indicates the prospects of using these photodiodes in the telecommunications range. In addition, the small width of the photosensitivity spectrum (0.12 μm) makes it possible to use such photodiodes to detect small signals during atmospheric signal transmission without the use of appropriate filters.

Figure 7 shows the volt-ampere characteristics characteristic of the studied photodiodes, measured in the temperature range 9–290 K.

A conclusion about the mechanism of the dark current flow can be made based on the type of temperature dependence of the photodiode VAC. In general form, the dependence of the volumetric dark current of the photodiode on the temperature can be described by the

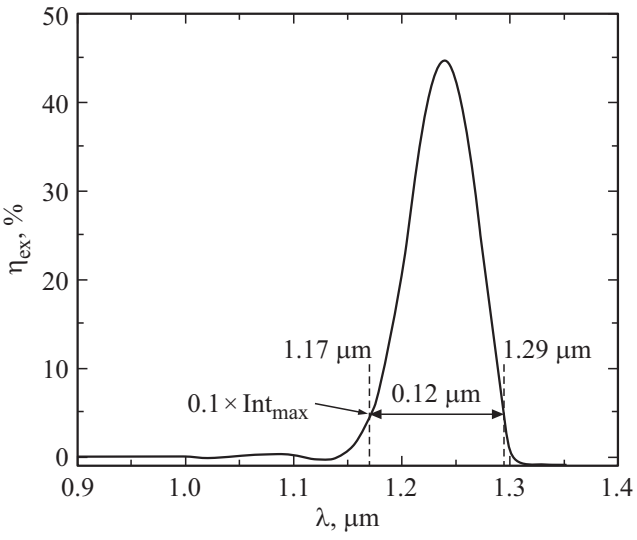

Figure 6. Spectral dependence of the external quantum output of photodiodes at room temperature.

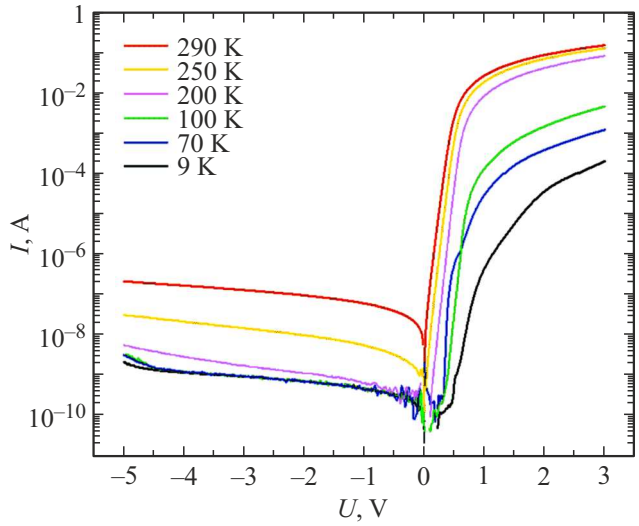

Figure 7. Typical photodiode VAC measured in the temperature range 9–290 K.

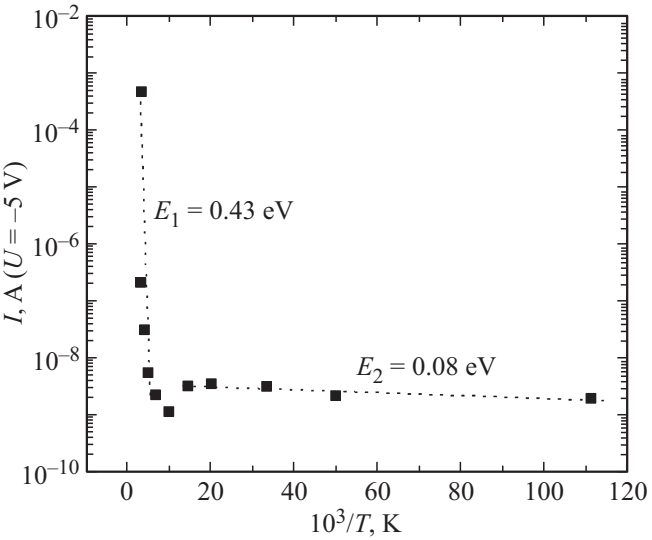

Figure 8. Dependence of the photodiode dark current on temperature at a fixed offset −5 V.

expression [17]

$$I = I_d e^{\frac{-E}{kT}}, \qquad (1)$$

where E — activation energy of the dark current flow mechanism, T — absolute temperature, k — Boltzmann constant. Figure 8 shows the dependence of the dark current of the photodiode at an offset of −5 B on the inverse temperature on a semi-logarithmic scale. The relative measurement error of the dark current was up to 10%.

Two temperature ranges can be distinguished based on this dependence: 200–290 and 9–200 K with activation energies of 0.43 and 0.08 eV, respectively. The calculations used the value of the band gap of the solid solution $In_{0.3}Ga_{0.7}As$ at room temperature $E_g = 1.01$ eV. Thus, the values of the activation energies are ∼ 50 and ∼ 10% of the band gap width of the solid solution comprising *p-n*-transition. The generation-recombination current mechanism of which is described below makes the strongest contribution to the dark current in the temperature range of 200–300 K. The total electric field in the space charge region (SCR) increases when the *p-n*-transition is reversed, and the equilibrium between the generation and recombination processes is violated in favor of carrier generation, which occurs through traps with energy levels near the middle of the band gap. The hole formed in the valence band is transferred by the electric field of the SCR to the *p*-region if thermal excitation leads to the casting of an electron from the valence band to the trap level. An electron localized on the trap cannot return to the valence band, since there are no holes with which it would recombine. As a result, there is a probability of thermal excitation of the electron into the conduction band of the SCR, from where it is transferred to the *n*-region. The current attributable to the tunneling of carriers through trap levels located in the band gap prevails at lower temperatures in the range of 9–200 K [18]. The sources of these levels may be defects that occur during the growth of epitaxial layers, or uncontrolled impurities.

4. Conclusion

New InGaAs photodiode structures based on a digital metamorphic buffer layer were formed on a GaAs substrate using the MOCVD. The use of the new MB layer design made it possible to create photodiodes for the range 1.17–1.29 μm with a low dark current. The dark current at room temperature and reverse offset ∼ 5 V was $2 \cdot 10^{-7}$ A for photodiodes with a mesastructure diameter of 560 μm, which corresponds to the current density of $8 \cdot 10^{-5}$ A/cm^2. Thus, the proposed design of a digital MB layer is promising for the formation of photosensitive structures for the wavelength range > 1 μm.

The study of the temperature dependence of the volt-ampere characteristics of photodiodes showed that the volume component of the reverse dark current contains two components: generation-recombination component, prevailing in the temperature range of 200–300 K, and tunnel component — in the range of 9–200 K.

Funding

This study was carried out with the support of the state assignment of the Ministry of Education and Science of the Russian Federation (project No. FSWR-2023-0037).

Acknowledgments

The authors express their gratitude to K.E. Kudryavtsev, an employee of the IFM RAS, for measuring the photoluminescence and stimulated radiation spectra.

Conflict of interest

The authors declare that they have no conflict of interest.

References

[1] Yang He, Yurun Sun, Yan Song, Yongming Zhao, Shuzhen Yu, Jianrong Dong. Jpn. J. Appl. Phys., **55**, 065501 (2016).
[2] Daehwan Jung, Patrick G. Callahan, Bongki Shin, Kunal Mukherjee, Arthur C. Gossard, John E. Bowers. J. Appl. Phys., **122**, 225703 (2017).
[3] N.A. Kalyuzhnyy, S.A. Mintairov, A.M. Nadtochiy, V.N. Nevedomskiy, D.V. Rybalchenko, M.Z. Shvarts. Electron. Lett., **53** (3), 173 (2017).
[4] Pamela Jurczak, Kimberly A. Sablon, Marina Gutiérrez, Huiyun Liu, Jiang Wu. Infr. Phys. Technol., **81**, 320 (2017).
[5] K. Swaminathan, L.-M. Yang, T.J. Grassman, G. Tabares, A. Guzman, A. Hierro, M.J. Mills, S.A. Ringel. Opt. Express, **19**, 7280 (2011).
[6] Yang Nan-Nan, Ma Ying-Jie, Gu Yi, Chen Xing-You, Gong Qian, Zhang Yong-Gang. J. Infrared Millim. Waves, **38** (3), 275 (2019).
[7] Zhu Bin, Han Qin, Yang Xiao-Hong, Ni Hai-Qiao, He Ji-Fang, NiuZhi-Chuan, Wang Xin, Wang Xiu-Ping, Wang Jie. Chinese Phys. Lett., **27** (3), 038504 (2010).
[8] S. Fedderwitz, A. Stohr, K.H. Tan, S.F. Yoon, Michael Weiss, ArturPoloczek, W.K. Loke, S. Wicaksono, Tien Khee Ng, V. Rymanov, A. Patra, E. Tangdiongga, Dieter Jäger. IEEE Phot. Techn. Lett., **21** (13), 911 (2009).
[9] X.Y. Chen, Y.G. Zhang, Y. Gu, L. Zhou, Y.Y. Cao, X. Fang, Hsby Li. J. Cryst. Growth, **393**, 75 (2014).
[10] X.Y. Chen, Y. Gu, Y.G. Zhang, Y.J. Ma, B. Du, J. Zhang, W.Y. Ji, Y.H. Shi, Y. Zhu. J. Cryst. Growth, **488**, 51 (2018).
[11] S.Q. Liu, Q. Han, B. Zhu1, X.H. Yang, H.Q. Ni, J.F. He, X. Wang, M.F. Li, Y. Zhu, J. Wang, X.P. Wang, Z.C. Niu. Appl. Phys. Lett., **98**, 201104 (2011).
[12] S.M. Plankina, O.V. Vikhrova, Yu.A. Danilov, B.N. Zvonkov, N.Yu. Kononova, A.V. Nezhdanov, I.Yu. Pashenkin. Semiconductors, **50**, 1539 (2016).
[13] Sudip Saha, Daniel T. Cassidy, D.A. Thompson. J. Appl. Phys., **113**, 124301 (2013).
[14] J. Groenen, R. Carles, G. Landa. Phys. Rev. B, **58** (16), 10452 (1998).
[15] S.N.G. Chu, S. Nakahara, K.E. Strege, W.D. Johnston, jr. J. Appl. Phys., **57**, 4610 (1985).
[16] P.V. Seredin, A.V. Glotov, V.E. Ternovaya, E.P. Domashevskaya, I.N. Arsentyev, L.S. Vavilova, I.S. Tarasov. Semiconductors, **45**, 1433 (2011).
[17] I.V. Samartsev, S.M. Nekorkin, B.N. Zvonkov, V.Ya. Aleshkin, A.A. Dubinov, I.J. Pashenkin, N.V. Dikareva, A.B. Chigineva. Semiconductors, **52** (12), 1564 (2018).
[18] A.V. Sorochkin V.S. Varavin, A.V. Predein, I.V. Sabinina, M.V. Yakushev. Semiconductors, **46**, 535 (2012).

Translated by A.Akhtyamov